Available online at www.sciencedirect.com
ScienceDirect
Chemical Physics Letters 440 (2007) 51–55
CHEMICAL PHYSICS LETTERS
www.elsevier.com/locate/cplett

Dissociation of energy-selected CH_3CN^+ in a region 15.1–16.5 eV: Vibrationally enhanced dissociation and mechanisms

Chuan-Keng Huang [a], I.-Feng Lin [b], Su-Yu Chiang [b,*]

[a] Department of Applied Chemistry, National Chiao Tung University, 1001, Ta Hsueh Road, Hsinchu 30010, Taiwan
[b] National Synchrotron Radiation Research Center, 101, Hsin Ann Road, Hsinchu Science Park, Hsinchu 30076, Taiwan

Received 17 January 2007; in final form 28 March 2007
Available online 12 April 2007

Abstract

Threshold photoelectron–photoion coincidence spectra of CH_3CN were measured in a region 15.1–16.5 eV. We observed a small vibrational enhancement on dissociation of CH_3CN^+ and obtained kinetic energy releases for channels $C_2HN^+ + H_2$ and $CH_2^+ + HCN$. The kinetic energies released in channel $C_2HN^+ + H_2$ are substantial; a linearly extrapolated dissociation threshold of 14.68 ± 0.01 eV agrees with a Gaussian-3 B3LYP prediction 14.70 eV for formation of $HCCN^+ + H_2$. In contrast, the small releases for channel $CH_2^+ + HCN$ agree with a statistical calculation. We describe a plausible dissociation mechanism with the Gaussian-3 B3LYP method to rationalize experimental results.

1. Introduction

Acetonitrile (CH_3CN) is the simplest aliphatic nitrile and a common chemical solvent. The determination of its thermochemical properties is thus essential for an understanding of its chemical behavior. Isomeric structures and interconversion mechanisms of CH_3CN^+ have also been the subject of numerous experimental investigations and theoretical calculations because the thermal internal energy of CH_3CN facilities the interconversion of CH_3CN^+ into other isomers upon ionization and because various CH_3CN^+ isomers are observed in the dissociative photoionization of larger nitriles [1–7].

In the dissociative photoionization of CH_3CN, the channel $CH_3CN^+ \rightarrow C_2H_2N^+ + H$ of least energy attracts researchers to investigate the isomeric structures of fragment $C_2H_2N^+$ to obtain related thermochemical data and to understand the dissociation mechanisms [8–11]. Based on experimental results and quantum-chemical calculations [3,9–11], the formation of cyclic $C_2H_2N^+$ from the dissociation of four stable CH_3CN^+ isomers – CH_3CN^+, CH_2CNH^+, CH_2NCH^+, and CH_3NC^+ – was proposed. Recently, Choe reinvestigated the dissociation of CH_3CN^+ to fragment $C_2H_2N^+$ with mass-analyzed ion kinetic energy spectrometry (MIKES) and performed density-functional theory (DFT) calculations; he reported a distribution of kinetic energy released in the dissociation and predicted a c-$C_2H_3N^+$ intermediate on the potential energy surface (PES) of dissociation for formation of c-$C_2H_2N^+$ [6].

Three other fragments – C_2HN^+, CH_3^+, and CH_2^+ – were identified in a region 11.9–20.0 eV with photoionization (PI) and electron impact (EI) methods, but their reported appearance energies (AE) show some scatter: 14.94 ± 0.02 [1], 15.29 ± 0.02 [11] and 15.7 eV [12] for CH_2^+. Moreover, the AE values are considered to be upper limits because of exit channel barriers and kinetic shifts [13,14]; structural identification of observed fragment ions and dissociation mechanisms are thus lacking. In the present work, we investigated the dissociation of energy-selected CH_3CN^+ in a region 15.1–16.5 eV with a threshold photoelectron–photoion coincidence (TPEPICO) technique and Gaussian-3 B3LYP (G3B3) calculations. We derived branching ratios for observed ions and average releases of kinetic energy for channels $C_2HN^+ + H_2$ and $CH_2^+ +$ HCN from the coincidence spectra. The dissociation of

* Corresponding author. Fax: +886 3 578 3813.
E-mail address: schiang@nsrrc.org.tw (S.-Y. Chiang).

0009-2614/$ - see front matter © 2007 Elsevier B.V. All rights reserved.
doi:10.1016/j.cplett.2007.04.010

CH_3CN^+ to form c-$C_2H_2N^+ + H$ in a region 15.1–15.5 eV shows a small vibrational enhancement. Plausible dissociation mechanisms for both channels $C_2HN^+ + H_2$ and $CH_2^+ + HCN$ and the structure of fragment C_2HN^+ are discussed with the aid of G3B3 calculations.

2. Experiments and calculations

We performed the coincidence measurements on the Seya–Namioka beamline at NSRRC in Taiwan. Photon energies with resolution 30 meV and photon flux $>10^9$ photons s^{-1} in a region 15–17 eV were selected with a monochromator (1 m; 1200 grooves mm^{-1}; slit width 0.12 mm). Absolute photon energies were calibrated within ±0.006 eV on measurement of Rydberg signals in the threshold photoelectron spectrum of Ar. The molecular beam/threshold photoelectron–photoion coincidence (MB/TPEPICO) system is described in detail elsewhere [15,16]. Briefly, a mixture of ~10% CH_3CN (Aldrich, ~98%) in He (>99.999%) at a total stagnation pressure ~150 Torr was expanded through a nozzle and two skimmers to form a cooled CH_3CN beam to be ionized in the ionization chamber. The threshold electrons produced were extracted with a dc field 100 V m^{-1} and analyzed with a threshold photoelectron spectrometer; the ions produced were extracted with an electric field 2100 V m^{-1} with a pulse of duration 30 μs on detecting a threshold electron or a randomly generated signal and analyzed with a time-of-flight mass spectrometer. A subtraction of the randomly generated coincidence spectrum from the electron-triggered coincidence spectrum yielded a true coincidence spectrum.

Molecular structures and energies of CH_3CN and species pertinent to this work were calculated with G3B3 method using the GAUSSIAN 2003 program [17]. The equilibrium structure of a stable species was fully optimized at the B3LYP/6-31G(d) level, and single-point calculations were performed at levels MP4/6-31G(d), QCISD(T)/6-31G(d), MP4/6-31+G(d), MP4/6-31G(2df,p), and MP2(full)/G3 large; additional energies include a spin–orbit correction, higher-level corrections and a zero-point vibrational energy (ZPVE) calculated from the B3LYP/6-31G(d) vibrational wavenumbers on scaling by 0.96. Transition structures for dissociation channels were located and confirmed with intrinsic reaction coordinate (IRC) calculations at the B3LYP/6-31G(d) level; all identified transition structures were verified to have only one imaginary vibrational wavenumber.

3. Results and discussion

3.1. Vibrational enhancement and dissociation channels

The coincidence mass spectra of CH_3CN were measured at 17 energies in the range 15.1–16.5 eV. Fig. 1a–d shows the corrected and normalized coincidence mass spectra of CH_3CN excited at 15.25, 15.43, 15.77, and 16.53 eV; solid lines indicate ion time-of-flight (TOF) signals fitted to Gaussian shapes. In the figures, ion signals corresponding to fragments – CH_3CN^+, c-$C_2H_2N^+$, C_2HN^+, CH_3^+ and CH_2^+ – were identified according to their flight durations and the vertical scale was expanded to show clearly the fragments C_2HN^+, CH_3^+ and CH_2^+. The remaining constant CH_3CN^+ signals at greater photon energies might be due to coincidences with hot electrons that result from autoionization of Rydberg states. We determined also the AE values 15.05 ± 0.03 eV for C_2HN^+ and 15.21 ± 0.08 eV for CH_2^+ from the onsets of their observed signals in the coincidence spectra; a discussion of fragment CH_3^+ is omitted because of its small abundance.

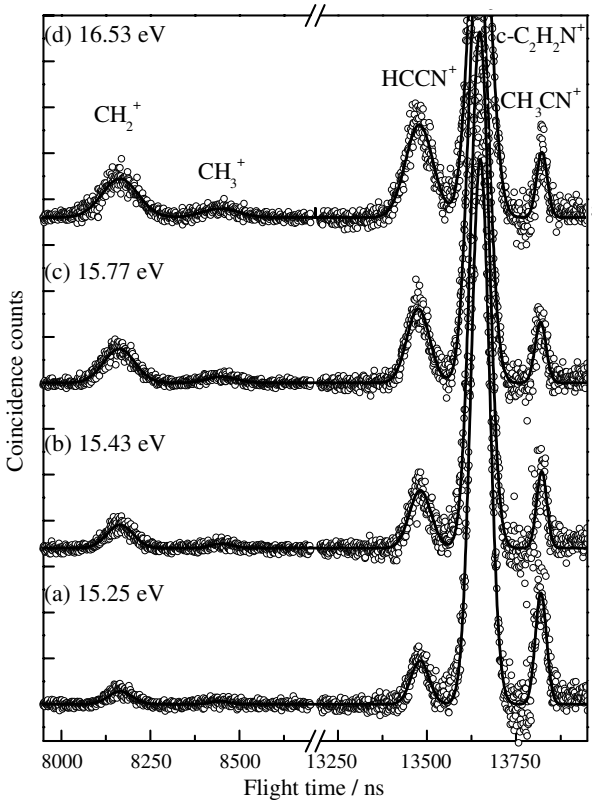

Fig. 1. Coincidence mass spectra of CH_3CN excited at photon energies: (a) 15.25, (b) 15.43, (c) 15.77 and (d) 16.53 eV.

A small vibrational enhancement on dissociation of CH_3CN^+ to form c-$C_2H_2N^+ + H$ was observed in a region 15.1–15.5 eV. Fig. 2a shows the branching ratios of CH_3CN^+ and c-$C_2H_2N^+$ in a region 15.1–15.5 eV with errors indicated; fractional abundances were obtained from the areas of the TOF peaks fitted to Gaussian profiles and errors were calculated from the standard deviations of the fitted TOF peaks. The errors for the branching ratios of CH_3CN^+ and c-$C_2H_2N^+$ are ~1% and ~0.2%, respectively; larger errors for CH_3CN^+ are due to their small signals. To show the vibrationally enhanced dissociation, Fig. 2b shows the original band and three vibrational bands of the second ionic excited state $\tilde{B}^2E$ of CH_3CN^+ in the threshold photoelectron spectrum. The origin at 15.14 eV and three vibrational bands at 15.25, 15.32, and 15.43 eV agree with values 15.133, 15.237, 15.311 and 15.414 eV

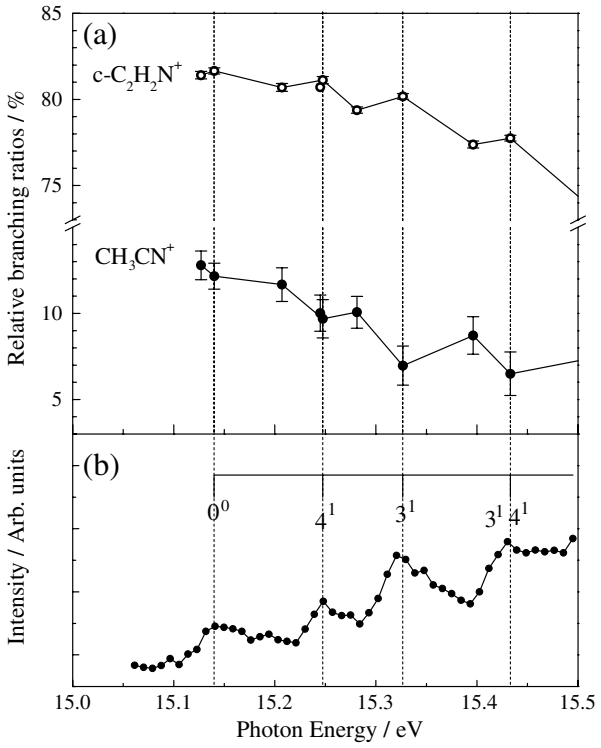

Fig. 2. (a) Branching ratios of CH_3CN^+ and c-$C_2H_2N^+$ in a region 15.10–15.5 eV with errors indicated. (b) Threshold photoelectron spectrum of CH_3CN to demonstrate the vibrationally enhanced dissociation of CH_3CN^+.

obtained from published photoelectron spectrum [18]; the three vibrational bands are attributed to excitations to the C–C stretching (v_4), symmetric CH_3 deformation (v_3), and combination ($v_3 + v_4$) modes, respectively. As seen in the figures, a notable decrease of CH_3CN^+ signals is accompanied with an increase of c-$C_2H_2N^+$ signals with excitation to 4^1, 3^1 and 3^14^1 vibrational levels. Because according to previous calculations a precursor c-$C_2H_3N^+$ is formed before dissociating to form c-$C_2H_2N^+$ [6], this enhancement indicates that excitation to these two vibrational modes of CH_3CN^+ facilitates H-migration and cyclization in the isomerization.

Table 1 lists G3B3 energies, E_0(G3B3), for CH_3CN, CH_3CN^+ isomers, and species pertinent to dissociation of CH_3CN^+ and energy differences, ΔE(G3B3), relative to CH_3CN to aid in understanding the dissociation properties. For fragment C_2HN^+, two dissociation channels $HCCN^+ + H_2$ and c-$HCCN^+ + H_2$ are energetically accessible based on comparison of the experimental AE value 15.05 ± 0.03 eV with their predicted reaction energies 14.70 and 14.88 eV; we discuss later a plausible C_2HN^+ structure based on the measured kinetic energies and predicted dissociation mechanism. A predicted reaction energy 14.91 eV for channel $CH_2^+ + HCN$ is smaller than the experimental AE value 15.21 ± 0.08 eV, likely because excess energies required in the dissociation to compete with other dissociation channels at smaller energies or to surmount reaction barriers.

Table 1
Calculated G3B3 energies, E_0(G3B3), for CH_3CN, CH_3CN^+ isomers, and species pertinent to dissociative photoionization of CH_3CN and energy differences, ΔE(G3B3), relative to CH_3CN

Species	Symmetry	E_0(G3B3) (hartree)	ΔE(G3B3) (eV)
CH_3CN	C_{3v}	−132.66316	0
CH_3CN^+	C_1	−132.21467	12.20
CH_2CNH^+	C_{2v}	−132.29933	9.90
CH_2NCH^+	C_{2v}	−132.28138	10.39
c-$C_2H_3N^+$	C_s	−132.23060	11.77
CH_3NC^+	C_{3v}	−132.20875	12.37
$HCCN^+$	C_s	−130.95699	
c-$HCCN^+$	C_s	−130.94870	
$HCNH^+$	$C_{\infty v}$	−93.64767	
CH_3^+	D_{3h}	−39.43137	
CH_2^+	C_{2v}	−38.73714	
HCN	$C_{\infty v}$	−93.37825	
CN	$C_{\infty v}$	−92.67788	
CH	$C_{\infty v}$	−38.45930	
H_2	$D_{\infty h}$	−1.16748	
H		−0.50109	
LM1	C_s	−132.19408	12.76
LM2	C_{2v}	−132.29931	9.90
LM3	C_{2v}	−132.26972	10.71
TS1	C_1	−132.18182	13.10
TS2	C_1	−132.18226	13.09
TS3	C_1	−132.14521	14.09
TS4	C_1	−132.11072	15.03

3.2. Average releases of kinetic energy and dissociation mechanisms

The C_2HN^+ and CH_2^+ signals fitted satisfactorily to Gaussian profiles have widths greater than those of CH_3CN^+ signals, reflecting releases of kinetic energy upon dissociation. In general, a reaction with a statistical product energy distribution will release the translational energy as a three-dimensional Maxwell–Boltzmann distribution and the resultant ion TOF distribution is a Gaussian function when the distribution projected along the detection axis [19]. Accordingly, the average release of kinetic energy is related to the full width at half maximum (fwhm) of the TOF peak and calculated from that fwhm according to the Maxwellian equation [20,21]

$$\langle \mathrm{KE} \rangle = \frac{3}{16 \ln 2} (e\varepsilon)^2 (\mathrm{fwhm})^2 \frac{M_\mathrm{p}}{M_\mathrm{f}(M_\mathrm{p} - M_\mathrm{f})} - \frac{3}{2} RT \times \frac{M_\mathrm{f}}{(M_\mathrm{p} - M_\mathrm{f})} \quad (1)$$

in which $e = 1.602 \times 10^{-19}$ C is the charge, $\varepsilon = 2100$ V m^{-1} is the strength of the pulsed electric field for ion extraction, M_p and M_f are masses of parent and fragment ions, and $T = 27$ K is the transverse temperature of the molecular beam calculated from fwhm 35 ns of CH_3CN^+ signals [21].

For channel $C_2HN^+ + H_2$, Fig. 3a shows the measured kinetic energies, a linear fit and QET calculations for formation of $HCCN^+$ and c-$HCCN^+$, depicted as circles, a solid line, a dashed curve, and a dashed–dotted curve, respectively. In the QET calculations according to an equa-

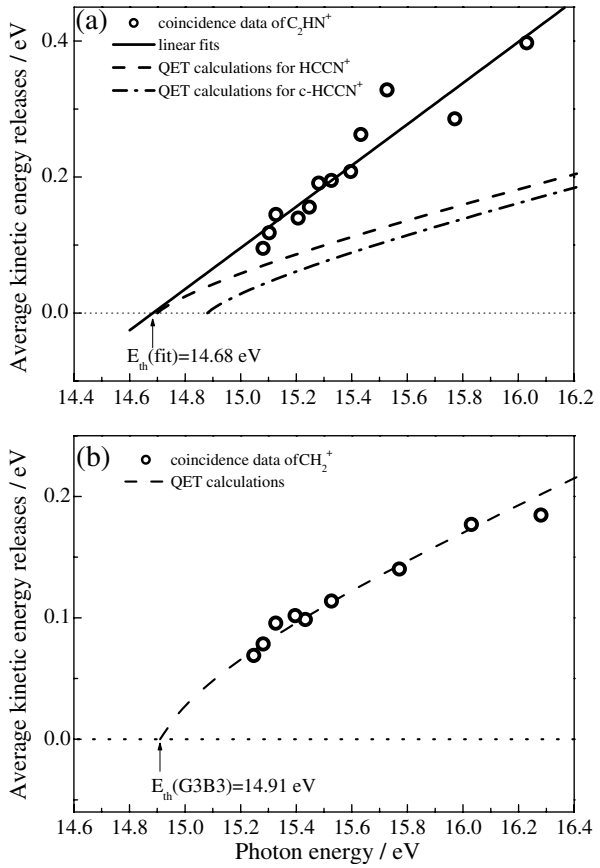

Fig. 3. Average kinetic energy released into dissociation channels $CH_3CN^+ \rightarrow$ (a) $C_2HN^+ + H_2$ and (b) $CH_2^+ + HCN$. In (a), data, a line fitted to data, and QET calculations for formation of $HCCN^+$ and c-$HCCN^+$ are marked as circles, solid line, dashed curve and dashed–dotted curve, respectively; in (b) data and QET calculations are marked as circles and dashed curve.

tion formulated by Klots [22–24], the G3B3 reaction energies 14.70 and 14.88 eV were taken as dissociation thresholds for formation of $HCCN^+$ and c-$HCCN^+$, respectively, and vibrational wavenumbers of 275, 867, 1235, 1887, 3166, and 185 cm^{-1} for $HCCN^+$ and 874, 1002, 1211, 1630, 3118, and 871 cm^{-1} for c-$HCCN^+$ were obtained from the B3LYP/6-31G(d) calculations on scaling 0.96. The predicted structure of $HCCN^+$ is quasi-linear with C_s symmetry; our predictions are lengths of 1.087, 1.293 and 1.211 Å for C–H, C–C and C–N bonds, respectively, and angles ∠HCC = 179.7° and ∠CCN = 179.3°. As seen in the figure, the experimental data are greater than both QET calculations, implying the presence of an exit barrier required for a structural alteration to form a transition state upon dissociation to form H_2. In addition, a dissociation threshold at 14.68 ± 0.01 eV obtained by linearly extrapolating coincidence data agrees satisfactorily with a G3B3 prediction 14.70 eV for channel $HCCN^+ + H_2$; fragment $HCCN^+$ instead of fragment c-$HCCN^+$ is accordingly the most likely structure.

For channel $CH_2^+ + HCN$, Fig. 3b shows the measured kinetic energies and QET calculations with a predicted G3B3 reaction energies 14.91 eV, depicted as circles and a dashed curve, respectively. In contrast to channel $HCCN^+ + H_2$, the experimental data agree satisfactorily with QET calculations. This result indicates that the energy required for H migration is smaller than the dissociation threshold and no significant exit barriers occurs during dissociation.

To explore further the dissociation mechanisms for both dissociation channels, we performed G3B3 calculations to obtain plausible transition states and intermediates in the reaction path that occurs off the ground electronic state surface of CH_3CN^+ with a assumption that internal conversion to the highly-excited $\tilde{X}^2E$ state occurs much more rapidly than direct dissociation from the initial excited $\tilde{B}^2E$ state. A feasible dissociation mechanism for channels $CH_2^+ + HCN$ and $HCCN^+ + H_2$ is shown in Fig. 4. In

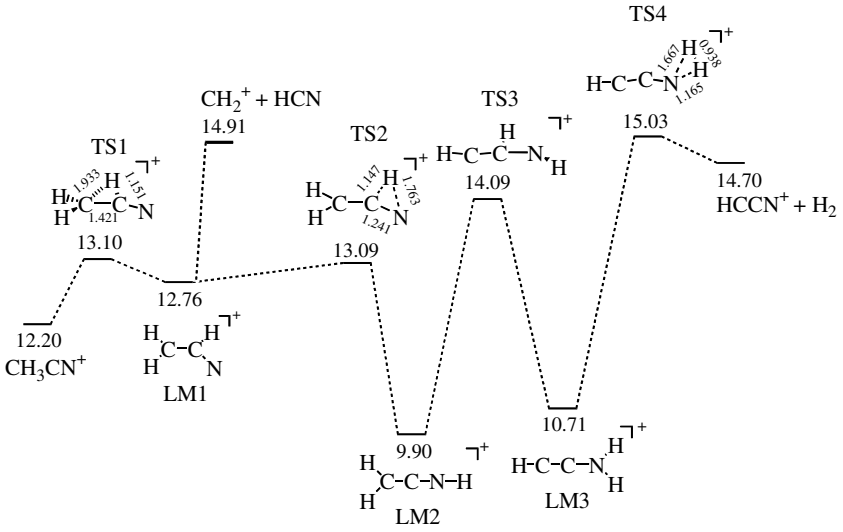

Fig. 4. Theoretical predictions of relative G3B3 energies in eV for the dissociation of CH_3CN^+ from the highly-excited ground electronic state to from $HCCN^+ + H_2$ and $CH_2^+ + HCN$; bond lengths in Å and interbond angles in ° are indicated for molecular structures optimized at the B3LYP/6-31G(d) level.

the figure, CH_3CN^+ first undergoes H migration via a cyclic transition state TS1 with a barrier at 0.9 eV to form an intermediate CH_2CHN^+ (LM1). This intermediate LM1 can proceed through a direct cleavage of the C–C bond to form $CH_2^+ + HCN$, resulting in a statistical energy distribution, compatible with experimental results. In contrast, intermediate LM1 can further proceed through H migrations from the CH and CH_2 groups to the N terminal via TS2 and TS3 with predicted barriers at 0.89 and 1.89 eV to form intermediates CH_2CNH^+ (LM2) and $CHCNH_2^+$ (LM3), respectively; the intermediate LM3 then dissociates through TS4 with a reverse barrier at 0.33 eV to form $HCCN^+ + H_2$. This dissociation mechanism supports the experimental observations of a non-statistical kinetic energy distribution.

We sought to form c-$HCCN^+$ from dissociation of $CHCNH_2^+$ (LM3) or c-CH_3CN^+, a dissociation precursor for formation of fragment c-CH_2CN^+, but located no transition state for either process. Channel c-$HCCN^+ + H_2$ is accordingly an unlikely dissociation channel based on the experimental results and G3B3 calculations.

4. Conclusion

The dissociative photoionization of CH_3CN was studied in a region 15.1–16.5 eV with a TPEPICO technique and G3B3 calculations. Dissociation of CH_3CN^+ shows a small vibrational enhancement and fragments C_2HN^+ and CH_2^+ are observed at 15.05 ± 0.03 and 15.21 ± 0.08 eV, respectively. From a comparison of a linearly extrapolated dissociation threshold at 14.68 ± 0.01 eV with a G3B3 prediction 14.70 eV for channel $HCCN^+ + H_2$, fragment $HCCN^+$ is the most likely structure; moreover, a predicted dissociation occurring off the ground electronic state surface of CH_3CN^+ and through a tight transition state supports the experimental observation of great kinetic energies released in the dissociation. In contrast, the dissociation to form $CH_2^+ + HCN$ through a local intermediate without an exit barrier supports the observation of a statistical distribution of kinetic energy.

Acknowledgement

National Synchrotron Radiation Research Center and National Science Council of Taiwan (Contract No. NSC95-2113-M-213-002) provided financial support for this work.

References

[1] V.H. Dibeler, K.S. Liston, J. Chem. Phys. 48 (1968) 4765.
[2] T. Pasinszki, H. Yamakado, K. Ohno, J. Phys. Chem. 99 (1995) 14678.
[3] P.M. Mayer, M.S. Taylor, M.W. Wong, L. Radom, J. Phys. Chem. A 102 (1998) 7074.
[4] C. Mair, J. Roithova, J. Fedor, M. Lezius, Z. Herman, T.D. Mark, Int. J. Mass Spectrom. 223 (2003) 279.
[5] G.d. Petris, S. Formarini, M.E. Crestoni, A. Troiani, P.M. Mayer, J. Phys. Chem. A 109 (2005) 4425.
[6] J.C. Choe, Int. J. Mass Spectrom. 235 (2004) 15.
[7] E.K. Chess, R.L. Lapp, M.L. Gross, Org. Mass Spectrom. 17 (1982) 475.
[8] J.L. Holmes, F.P. Lossing, P.M. Mayer, Chem. Phys. Lett. 212 (1993) 134.
[9] P.W. Harland, R.G.A.R. Maclagan, H.F. Schaefer III, J. Chem. Soc. Frarday Trans. II 85 (1989) 187.
[10] D.J. Swanton, G.B. Bacskay, G.D. Willett, N.S. Hush, J. Mol. Struct. (THEOCHEM) 91 (1983) 313.
[11] D.M. Rider, G.W. Ray, E.J. Darland, G.E. Leroi, J. Chem. Phys. 74 (1981) 1652.
[12] M.A. Haney, J.L. Franklin, J. Chem. Phys. 48 (1968) 4093.
[13] B.P. Tsai, T. Baer, A.S. Werner, S.F. Lin, J. Phys. Chem. 79 (1975) 570.
[14] H. Shiromaru, Y. Achiba, K. Kimura, Y.T. Lee, J. Phys. Chem. 91 (1987) 17.
[15] Y.-S. Fang, I.-F. Lin, Y.-C. Lee, S.-Y. Chiang, J. Chem. Phys. 123 (2005) 054312.
[16] S.-Y. Chiang, C.-I. Ma, J. Phys. Chem. A 104 (2000) 1991.
[17] M.J. Frisch, et al., Gaussian, Inc., Pittsburgh, PA, 2003.
[18] M. Gochel-Dupuis, J. Delwiche, M.-J. Hubin-Franskin, J.E. Collin, Chem. Phys. Lett. 193 (1992) 41.
[19] T. Baer, W.L. Hase, Unimolecular Reaction Dynamics: Theory and Experiments, Oxford University Press, New York, 1996, p. 160.
[20] T. Baer, G.D. Whillett, D. Smith, J.S. Phillips, J. Chem. Phys. 70 (1979) 4076.
[21] R. Stockbauer, Int. J. Mass Spectrom. Ion Phys. 25 (1977) 89.
[22] C.E. Klots, J. Chem. Phys. 58 (1973) 5364.
[23] C.E. Klots, Adv. Mass Spectrom. 6 (1974) 969.
[24] C.E. Klots, J. Chem. Phys. 64 (1976) 4269.